



Wetting of molten Sn–3.5Ag–0.5Cu on Ni–P(–SiC) coatings deposited on high volume fraction SiC/Al composite

Xiang-zhao ZHANG¹, Xiao-lang WU¹, Gui-wu LIU¹,
Wen-qiang LUO¹, Ya-jie GUO², Hai-cheng SHAO¹, Guan-jun QIAO^{1,3}

1. School of Materials Science and Engineering, Jiangsu University, Zhenjiang 212013, China;

2. School of Materials Science and Engineering, Chang'an University, Xi'an 710064, China;

3. State Key Laboratory for Mechanical Behavior of Materials, Xi'an Jiaotong University, Xi'an 710049, China

Received 24 May 2017; accepted 30 October 2017

Abstract: The wetting of molten Sn–3.5Ag–0.5Cu alloy on the Ni–P(–SiC) coated SiC_p/Al substrates was investigated by electroless Ni plating process, and the microstructures of the coating and the interfacial behavior of wetting systems were analyzed. The SiC particles are evenly distributed in the coating and enveloped with Ni. No reaction layer is observed at the coating/SiC_p/Al composite interfaces. The contact angle increases from ~19° with the Ni–P coating to 29°, 43° and 113° with the corresponding Ni–P–3SiC, Ni–P–6SiC and Ni–P–9SiC coatings, respectively. An interaction layer containing Cu, Ni, Sn and P forms at the Sn–Ag–Cu/Ni–P–(0,3,6)SiC coated SiC_p/Al interfaces, and the Cu–Ni–Sn and Ni–Sn–P phases are detected in the interaction layer. Moreover, the molten Sn–Ag–Cu can penetrate into the Ni–P(–SiC) coatings through the Ni–P/SiC interface and dissolve them to contact the SiC_p/Al substrate.

Key words: Ni coating; Sn–Ag–Cu alloy; SiC_p/Al composite; wetting; microstructures; interface

1 Introduction

The SiC particles reinforced Al matrix (SiC_p/Al) composite is provided with many distinct advantages, including high thermal conductivity (CT), low weight, low and tailorable coefficient of thermal expansion (CTE), as well as appropriate mechanical properties, which are well suited to the requirement of advanced electronic packaging fields, like heat sinks, substrate and the baseplates of various power modules [1–3].

Joining is an indispensable process for application of the high volume fraction (HFC) SiC_p/Al composites in the electronic packaging. Among a variety of joining techniques, brazing is the most commonly adopted one for relatively low heating temperature, material deformation, residual stress and stable performance, etc. However, it is complicated and difficult to directly braze the SiC_p/Al composite due to the presence of the tenacious and chemically stable Al₂O₃ film and the

exposed SiC particles on the surface of SiC_p/Al composite [4,5]. To overcome the defects as mentioned above, an attempt is made to fabricate a metallic layer on the surface of the SiC_p/Al composite by the electroless plating to enhance the wettability, which is widely used for surface modification of the SiC_p/Al composite due to the advantages of uniform thickness, low-cost, excellent corrosion resistance and thermal stability [6–8].

Recently, the co-deposition of SiC particles on different substrates (such as Al, Mg alloys and steel) in the electroless Ni plating process was proposed, while these reports were mainly focused on the wear and corrosion resistances [9–13]. For instance, CALDERON et al [11] investigated the erosion–corrosion behavior of Ni–P–SiC composite coatings on carbon steel, and found that the incorporation of SiC nanoparticles can improve the microhardness and erosion–corrosion resistance of the composite coatings compared with the Ni–P coatings. However, the effect of SiC additions on the wetting and interfacial behavior of Sn-based alloys on the Ni–P

Foundation item: Projects (51572112, 51401034) supported by the National Natural Science Foundation of China; Project (BK20151340) supported by the Natural Science Foundation of Jiangsu Province, China; Projects (2014-XCL-002,TD-XCL-004) supported by the Six Talent Peaks Project of Jiangsu Province, China; Project (BRA2017387) supported by the 333 Talents Project of Jiangsu Province, China; Project ([2015]26) supported by the Innovation/Entrepreneurship Program of Jiangsu Province, China; Project ([2016]15) supported by the Qing Lan Project, China

Corresponding author: Gui-wu LIU; Tel: +86-15952898923; E-mail: gwliu76@ujs.edu.cn
DOI: 10.1016/S1003-6326(18)64822-8

coating has not been reported, although the wetting of Sn-based alloys on the Ni–P coating was investigated [14–18]. LIN et al [17] surveyed the wettability of three commercial solder pastes (Sn–3.5Ag, Sn–37Pb and Sn–3.5Ag–0.5Cu) on electroplated Ni–P coating with various concentrations of phosphorous, showing that the wettability was enhanced with the increase of phosphorous in the Ni–P coating.

Based on the facts that the SiC additions in the Ni–P coating can contribute to decrease the difference of CTE between the coating and the SiC_p/Al composite substrate and improve the adhesion of the coating to the substrate to a certain extent (reported in our another paper) [19]. In this work, the SiC particles were incorporated (in various contents) in the Ni–P coating by a composite plating process, and the surface and cross-sectional morphologies, coating phase composition and surface roughness of the Ni–P(–SiC) coated HFC SiC_p/Al composites were investigated. Moreover, the wetting and interfacial behavior of molten Sn–3.5Ag–0.5Cu on the Ni–P(–SiC) coated SiC_p/Al composites and SiC ceramic, performed by sessile drop tests, were also investigated and analyzed. Actually, this investigation on wetting of this system can contribute to transform from Pb-containing to Pb-free solder in the electronic package field.

2 Experimental

Commercial SiC_p/Al composite with 70% (volume fraction) SiC for electronic packaging (Xian MIQAM Microelectronic Materials Co., Ltd.) was used as the substrate in this experiment. The SiC_p/Al composite was cut into sheets with dimensions of $d/16 \text{ mm} \times (3-5) \text{ mm}$, and then ground to a plane by automatic grinding machine using the sequence 200, 400, 800 and 1500 mesh diamond grinding plates. The sheet samples were further ultrasonically cleaned with acetone for 10 min and subsequently rinsed with deionized water for subsequent electroless plating. The sizes of SiC particles added into electroless plating solution displayed a bimodal distribution of ~ 5 and $0.4 \mu\text{m}$. The SiC particles were pretreated by cleaning with hydrochloric acid at a concentration of 1:1 for 24 h to remove metal impurities and rinsing with distilled water, and finally dried before adding into the plating solution.

Prior to metal plating, the SiC_p/Al composite

substrate was sensitized, activated and then rinsed with distilled water in turn [8]. Table 1 lists the chemical composition of the composite electroless plating solution and the process parameters. To keep the SiC particles suspending in the solution, a magnetic stirring was adopted [10,13]. After the composite electroless plating, the Ni–P, Ni–P–3SiC, Ni–P–6SiC and Ni–P–9SiC coatings on the SiC_p/Al composite were obtained, here the four coatings correspond to the ones with SiC particle concentrations of 0, 3, 6 and 9 g/L in the plating solution, respectively. The Sn–3.5Ag–0.5Cu (mass fraction, %) samples for the sessile drop tests were cut from a Sn–3.5Ag–0.5Cu wire of $d/2 \text{ mm}$ and then curled up into a ball of 0.050 g for each wetting experiment. The wetting and spreading were evaluated by a high temperature contact angle measuring instrument (OCA15LHT–SV, Dataphysics, Germany). As soon as a spherical droplet was formed after the drop melting, the wetting process was recorded at a speed of 17 frames per second using a camera through a side-view window of the chamber. All the captured drop profiles were analyzed using drop-analysis software to obtain the average value of the left and right contact angles. The sessile drop tests of the Sn–3.5Ag–0.5Cu alloy on the Ni–P(–SiC) coated SiC_p/Al composites and SiC ceramic were performed at 400 °C for 30 min in a vacuum of $\sim 6 \times 10^{-4} \text{ Pa}$, and the heating rate was 5 °C/min.

The surface and cross-sectional microstructures and chemical compositions of the Ni–P(–SiC) coatings were examined and analyzed using scanning electron microscopy (SEM) coupled with energy dispersive spectroscopy (EDS). The EDS analysis was conducted to evaluate the surface element compositions of Si, P and Ni in the deposition layer, and the contents of SiC of the Ni–P(–SiC) coatings were determined from the Si content. The phase structures of the Ni–P(–SiC) coatings were identified by grazing incidence X-ray diffraction (GIXRD) and the angle of incidence was fixed at 2°. The surface morphologies of the Ni–P(–SiC) coatings were observed by an atomic force microscope (AFM, MFP-3D) in contact model with Bruker AFM probe (NCHV, 0.01–0.025 Ohm-cm antimony (*n*)-doped silicon, cantilever thickness of 3.5 μm , tip radius of 8 nm). After the wetting experiments, the solidified sessile drop/substrate couples were cross-sectioned, polished, and observed to investigate the interactions of the molten Sn–3.5Ag–0.5Cu and the Ni–P(–SiC) coatings.

Table 1 Chemical composition of electroless plating solution and process parameters

$\rho(\text{Na}_3\text{C}_6\text{H}_5\text{O}_7 \cdot 2\text{H}_2\text{O})/(\text{g} \cdot \text{L}^{-1})$	$\rho(\text{NiSO}_4 \cdot 6\text{H}_2\text{O})/(\text{g} \cdot \text{L}^{-1})$	$\rho(\text{NaH}_2\text{PO}_2 \cdot \text{H}_2\text{O})/(\text{g} \cdot \text{L}^{-1})$	$\rho(\text{CH}_3\text{COONa})/(\text{g} \cdot \text{L}^{-1})$	$\rho(\text{C}_3\text{H}_6\text{O}_3)/(\text{g} \cdot \text{L}^{-1})$
15	30	30	15	30
$\rho(\text{SiC})/(\text{g} \cdot \text{L}^{-1})$	Agitation speed/($\text{r} \cdot \text{min}^{-1}$)	Temperature/°C	pH	Plating duration/min
0, 3, 6 and 9	400–500	90	4.6	30

3 Results and discussion

3.1 Ni–P(–SiC) coatings

Figure 1 shows the surface SEM and AFM micrographs of the Ni–P(–SiC) coatings on the SiC_p/Al

composite. The surface of the SiC_p/Al composite is covered entirely with a dense and uniform Ni–P coating, and no obvious defects are observed on the surface of coating (Fig. 1(a)). A large number of fine globular nodules and no obvious aggregations of SiC particles are observed on the surfaces, leading to relatively rough

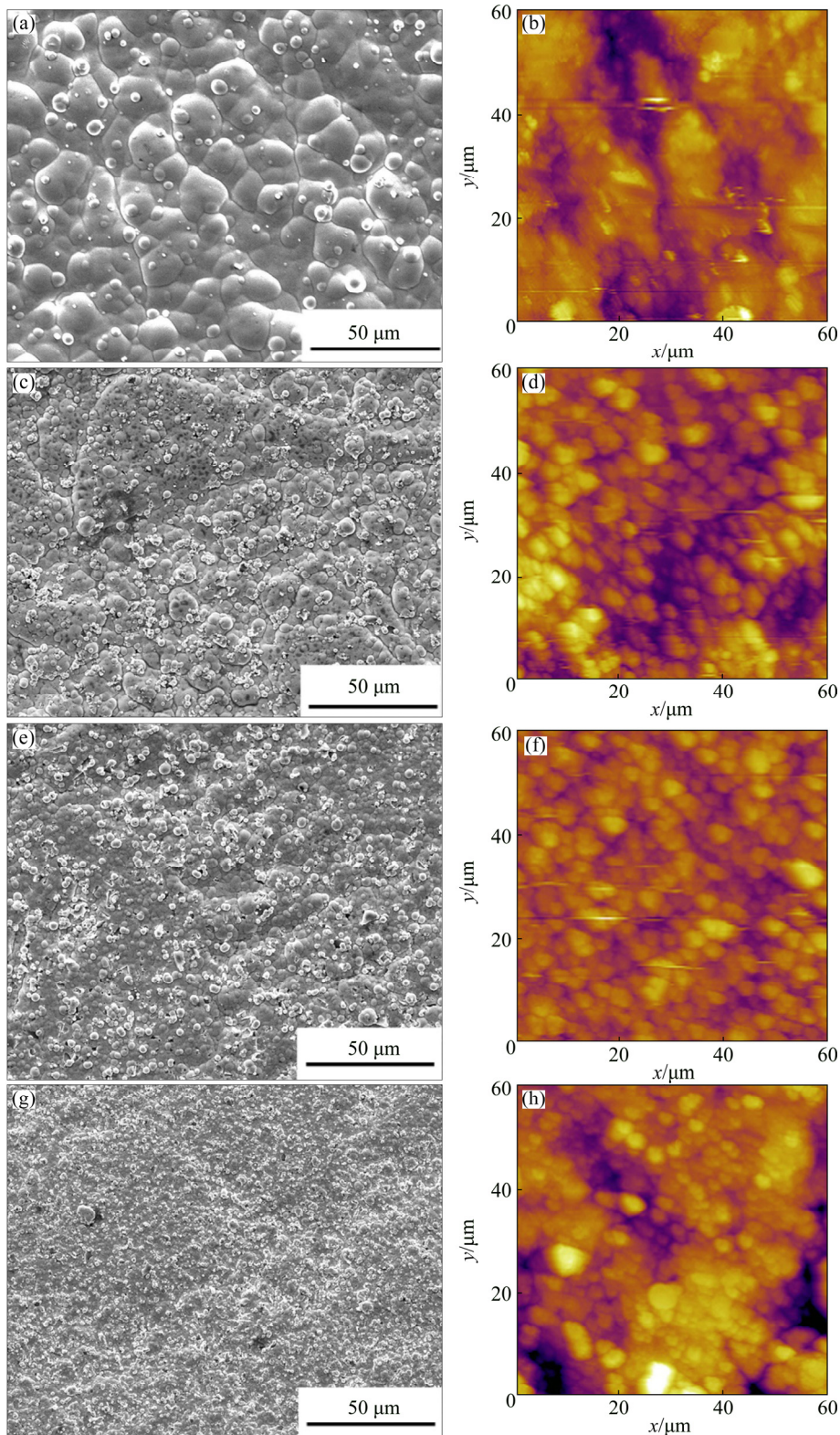


Fig. 1 Surface SEM (a, c, e, g) and AFM (b, d, f, h) micrographs of Ni–P(–SiC) coatings on SiC_p/Al composite deposited by adding SiC particles of 0 g/L (a, b), 3 g/L (c, d), 6 g/L (e, f) and 9 g/L (g, h) in plating solution

surfaces (Figs. 1(c)–(h)). Moreover, the SiC particle additions have an evident effect on the surface morphology of the coating. It is clear that the size of globular nodules decreases with the SiC concentration increasing from 0 to 3, 6 and 9 g/L. This phenomenon was also observed in similar systems [20–22]. What's more, it confirms the fact that the SiC particles that entered and homogeneously dispersed in the composite coatings increase the number of nuclei for the nucleation of nickel grain and inhibit its grain growth.

Figure 2 shows a typical cross-sectional SEM morphology of Ni–P–9SiC coated SiC_p/Al composite and the elemental EDS profiles across the Ni–P–9SiC/SiC_p/Al interface. It can be seen that the ~15 μm-thick coating can adhere tightly to the SiC_p/Al substrate and the SiC particles are evenly distributed in the coating and enveloped with nickel. According to the EDS result, the coating/substrate interface is clean and no obvious reaction layer is detected.

Figure 3 shows that the SiC content on the coatings and the arithmetic mean surface roughness (R_a) of the coatings as a function of the SiC concentration in the bath. As shown in Fig. 3(a), the SiC content on the coatings increases from 0 to 6.1%, 10.5%, 12.1% (mass

fraction) with the SiC concentration in the bath increasing from 0 to 3, 6, 9 g/L, respectively, and the increment of the SiC content significantly decreases when the SiC concentration is more than 6 g/L. During the electroless plating, the deposition of SiC particles on the coating surface accelerates accordingly with the increase of effective concentration of SiC particles in the bath due to the agitating action. However, the floatability of SiC particles is weakened as the SiC concentration increases to a certain extent because of the mass increase of partial SiC particles originated from aggregation of fine SiC particles. From Fig. 3(b), it is revealed that the surface roughness sharply increases from ~97 to 419 nm when the SiC concentration climbs from 0 to 3 g/L, while it increases slowly when the SiC concentration is higher than 3 g/L.

Figure 4 shows the GIXRD patterns of the Ni–P(–SiC) coatings on the SiC_p/Al composite. The XRD patterns exhibit a broad amorphous peak (at around $2\theta=45^\circ$), which is designated as the amorphous Ni in the coatings [20,23,24]. Moreover, some sharp peaks corresponding to the crystalline SiC are detected, and the SiC crystal peak intensity increases with the increase of SiC concentration.

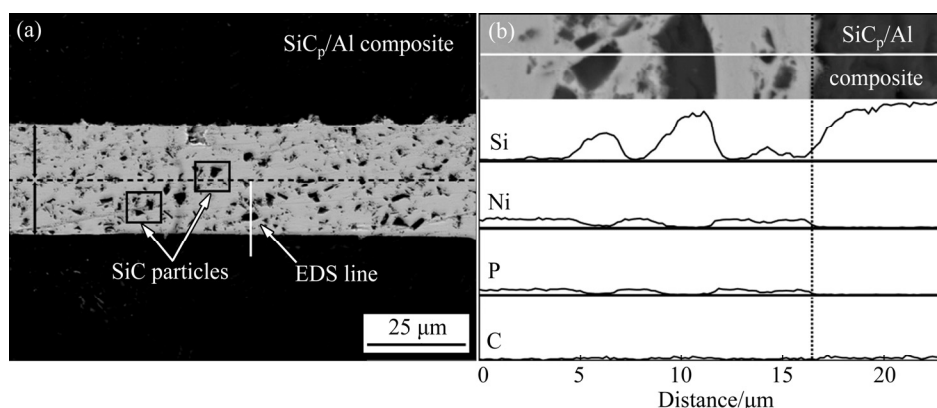


Fig. 2 Cross-sectional SEM image (a) and elemental EDS profiles (b) of Ni–P–9SiC coated SiC_p/Al sample ((a) is derived from two cross-sectional samples)

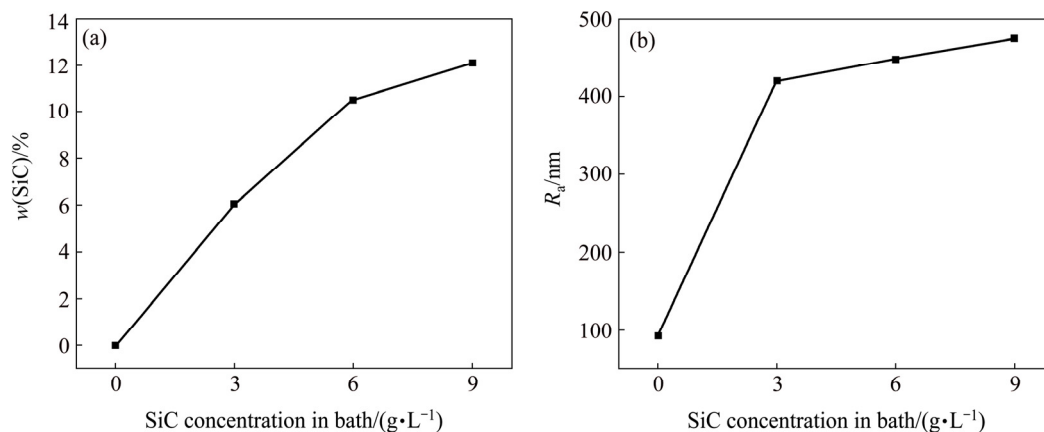


Fig. 3 Variations of SiC content (a) and arithmetic mean surface roughness (b) of coatings as function of SiC concentration in bath

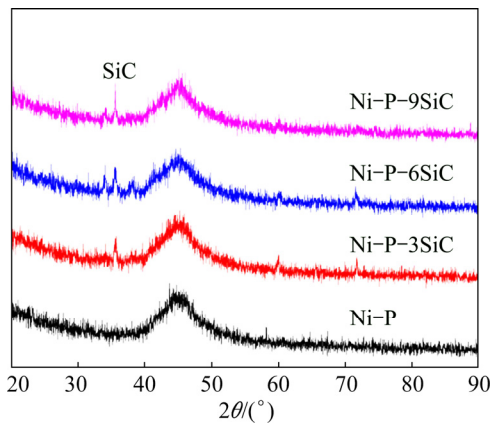


Fig. 4 GIXRD patterns of as-received Ni-P(-SiC) coatings on SiC_p/Al composite

3.2 Wetting and interfacial behavior

Figure 5 shows the wetting curves of molten Sn-3.5Ag-0.5Cu on the Ni-P(-SiC) coated SiC_p/Al composites and SiC ceramic after holding for 30 min at 400 °C and the photographs of solidified drops formed at the final states, and Table 2 presents the final contact angles. For the Sn-3.5Ag-0.5Cu/Ni-P coating system, the contact angle curve can be separated into three parts: I, II and III. At the beginning of the spreading stage (I), the contact angle decreases rapidly from ~100° at 300 °C to ~40° at 330 °C, and then the contact angle declines with the temperature increasing to the holding temperature (400 °C, stage II). After holding for ~500 s at 400 °C, the spreading arrives at the equilibrium with the contact angle of ~19° (stage III). The spreading rates in the three stages fall from $\sim 1.3 \times 10^{-1}$, to $\sim 2.1 \times 10^{-2}$ and 5.7×10^{-4} (°)/s, respectively. For the Sn-3.5Ag-0.5Cu/Ni-P-(3,6)SiC (i.e. Ni-P-3SiC and Ni-P-6SiC) coating systems, their initial spreading rates are far slower than that of Sn-3.5Ag-0.5Cu/Ni-P coating system, and no high speed spreading stage can be observed. Both the two wetting systems cannot reach the equilibrium after

holding for 1800 s at 400 °C. However, for the Sn-3.5Ag-0.5Cu/Ni-P-9SiC coating system, a spherical droplet is formed with contact angle of over 155° while reaching the melting temperature of 300 °C. Then, the contact angle declines slowly as the temperature increases. After holding for 1800 s at 400 °C, this system reaches the no-wetting equilibrium with the contact angle of ~113°.

In short, the SiC additions have a great effect on the final contact angle, that is the final contact angle increases from 19° to 29°, 43° and 113° with the SiC additions increasing from 0 to 3, 6, and 9 g/L, respectively (Table 2). In particular, a non-wetting phenomenon is observed as the SiC concentration is 9 g/L. Furthermore, it is obviously observed from the image of Sn-3.5Ag-0.5Cu/SiC couple that the Sn-based alloy does not wet the SiC substrate entirely and SiC has a strongly non-wetted surface ($\theta \approx 161^\circ$).

For high temperature wetting, it has long been known that both the surface roughness and the interface reaction have a profound and technologically important influence on the wetting and spreading behavior. In terms of the relationship between the surface roughness and the contact angle, WENZEL [24] discussed the effect of roughness on wetting behavior, and predicted that the apparent contact angle decreases with the roughness increasing if the contact angle is less than 90° [25]. Obviously, it is not agreement with the present experimental results. This discrepancy is mainly derived from the unreactive SiC particles in the coating as a series of energy barriers that the molten Sn-3.5Ag-0.5Cu drops must be overcome. According to the reactive production control (RPC) model, the wetting in reactive systems is governed by the final interfacial chemistry at the triple line [26,27]. Thus, a further investigation on the interface interactions between the drop and the coatings is carried out.

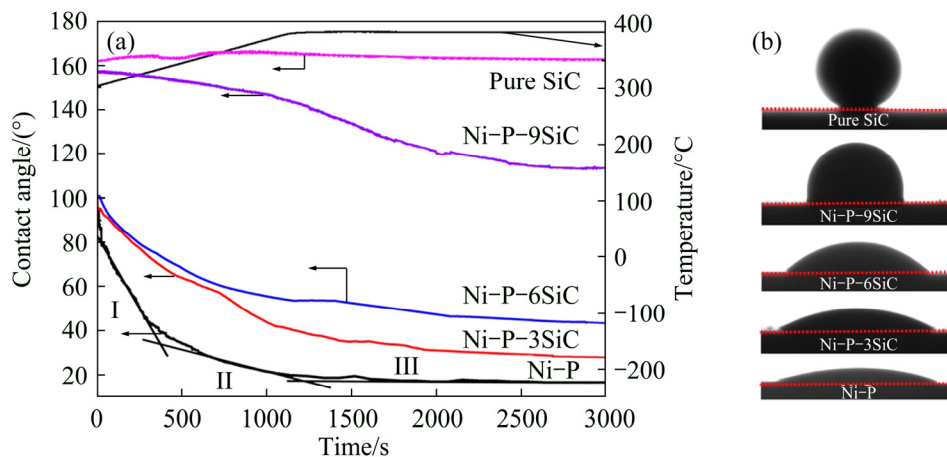


Fig. 5 Wetting curves (a) and sessile drop photographs (b) of molten Sn-3.5Ag-0.5Cu on Ni-P(-SiC) coated SiC_p/Al composites

Table 2 Contact angles of molten Sn–3.5Ag–0.5Cu on Ni–P(–SiC) coated SiC_p/Al composite

Metal/coated composite system	Contact angle/(°)
Sn–3.5Ag–0.5Cu/Ni–P	19
Sn–3.5Ag–0.5Cu/Ni–P–3SiC	29
Sn–3.5Ag–0.5Cu/Ni–P–6SiC	43
Sn–3.5Ag–0.5Cu/Ni–P–9SiC	113
Sn–3.5Ag–0.5Cu/SiC	161

Figure 6 shows the cross-sectional SEM images of the Sn–3.5Ag–0.5Cu/Ni–P(–SiC) coated SiC_p/Al systems and two typical schematic diagrams of interface structures. For the Sn–3.5Ag–0.5Cu/Ni–P coated SiC_p/Al system, the Ni–P coating is completely dissolved in the molten Sn–3.5Ag–0.5Cu drop after the wetting to form an interaction layer at the interface (Fig. 6(a)). Two kinds of phases (marked as Cu–Ni–Sn and

Ni–Sn–P) are observed in the interaction layer with thickness of ~40 μm, as shown in Fig. 6(b). As confirmed by the EDS analysis, the chemical compositions (mole fraction, %) of the two phases are 44.2Sn–32.4Cu–23.4Ni and 50.5Ni–26.0Sn–23.5P. According to the works reported [28–32], the gray phase is (Cu,Ni)₆Sn₅ and the dark Ni–Sn–P layer should be composed of Ni₃Sn₄ and Ni₃P phases. Besides the spreading kinetics and the final contact angles (Fig. 5), no significant difference is observed in the interaction layer when the lower-concentration (3 and 6 g/L) SiC particles are added in the Ni–P coating as shown in Figs. 6(c)–(f). The Ni–P–(3,6)SiC coatings are also completely consumed in the Sn–3.5Ag–0.5Cu drop after the wetting. Similarly, the two interaction layers with respective thicknesses of ~40 and 50 μm consist of the gray and dark phases. However, the thickness of the interaction layer is sharply decreased to ~20 μm when

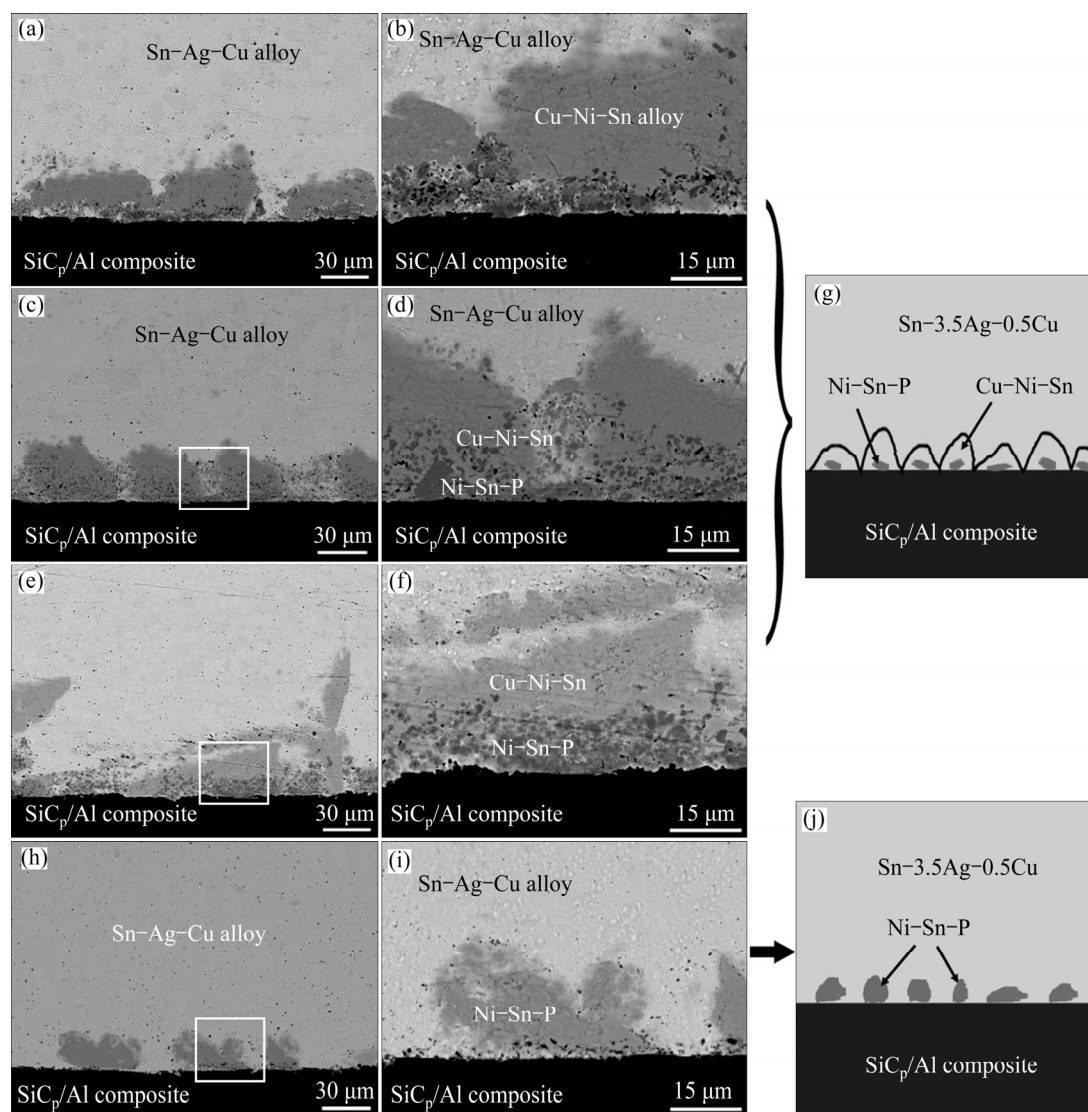


Fig. 6 Cross-sectional SEM images (a, b, c, d, e, f, h, i) of Sn–3.5Ag–0.5Cu/Ni–P(–SiC) coated SiC_p/Al couples and two typical schematic diagrams of interface structures (g, j): (a, b) Ni–P; (c, d) Ni–P–3SiC; (e, f) Ni–P–6SiC; (h, i) Ni–P–9SiC

the SiC concentration is 9 g/L, as shown in Figs. 6(h) and (i). The further EDS analysis confirms that the composition (mole fraction, %) of the only gray phase (Ni–Sn–P) between the drop and the substrate is mainly 50.2Ni–23.4P–26.4Sn, and that this Ni–Sn–P layer is thicker than that formed in other systems. Moreover, the molten Sn–Ag–Cu alloy can penetrate into the Ni–P(–SiC) coatings through the Ni–P/SiC interface and dissolve them to contact the SiC_p/Al substrate.

The constituent elements in the molten drop and the Ni–P(–SiC) coatings start to interdiffuse when the molten Sn–3.5Ag–0.5Cu drop contacts the coatings on the SiC_p/Al composite. The Ni₃Sn₄ nucleates firstly in the metastable rich-Ni coating near the drop/coating interface as the solubility of Ni in the molten Sn-based drops is very low. Subsequently, the ternary metallic compound (Cu,Ni)₆Sn₅ begins to nucleate due to the diffusion of Ni into the drop and the presense of Cu in the molten drop. Furthermore, the growth rate of (Cu,Ni)₆Sn₅ is much faster than that of the Ni₃Sn₄ [28,31], which is confirmed in this work (Figs. 6(a)–(f)). The P is remained in the original Ni–P(–SiC) coating accompanying with the consumption of Ni, resulting in formation of Ni₃P phase at the interface. However, the Cu–Ni–Sn layer (i.e., the (Cu,Ni)₆Sn₅ phase) cannot be observed in the Sn–3.5Ag–0.5Cu/Ni–P–9SiC coated SiC_p/Al system, which could be attributed to the increasing nucleation of Ni₃Sn₄ due to the improvement of SiC content, resulting in much more consumption of Ni in the Ni–P–9SiC coating. In addition, it is noted that no Ag element is observed in the interaction layers, that is, Ag is hardly involved in the interfacial interactions.

3.3 Wetting behavior

Apparently, the key point for the discussion given in next paragraphs is that the Ni–P–SiC coatings can be considered to be a dual-phase substrate in the Sn–3.5Ag–0.5Cu/Ni–P(–SiC)/SiC_p/Al wetting systems. The Cassie's equation is generally used to explain a composite contact angle (θ) on the heterogeneous surfaces consisting of B particles dispersed in a continuous A phase by a non-reactive liquid [33]:

$$\cos \theta = f_A \cos \theta_A + f_B \cos \theta_B \quad (1)$$

where f_A and f_B represent the surface fractions occupied by the surface phases A and B with contact angle θ_A and θ_B , respectively.

The surface fractions of the SiC particles in Ni–P–SiC coatings can be estimated by the SiC content on the coatings. So, we can obtain the relationship between the theoretical contact angle and the SiC content, as shown in Fig. 7. However, the variation in contact angle of Sn–3.5Ag–0.5Cu on the Ni–P(–SiC) composite

coatings is greatly inconsistent with the trend predicated by the Cassie's equation (Fig. 7). A possible reason for this disagreement is that the interfacial reaction products replace the Ni–P. As presented in Figs. 6(a)–(h), for the Ni–P–SiC coating with SiC content ($w(\text{SiC}) \leq 10.5\%$) the reaction product in contact with the molten drop is Cu–Ni–Sn, while the reaction product is Ni–Sn–P when $w(\text{SiC}) = 12.1\%$.

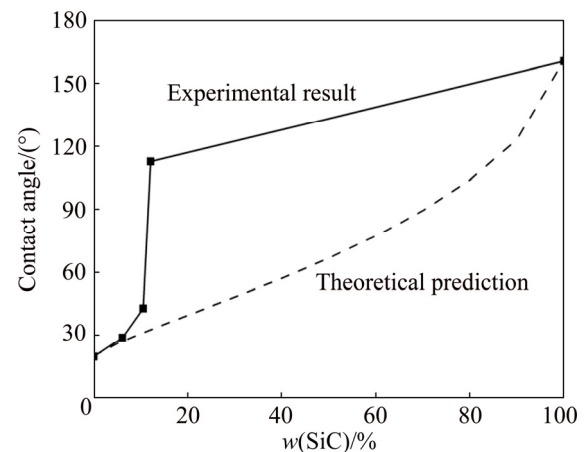


Fig. 7 Comparison between experimental result and theoretical prediction by Cassie's equation

For reactive wetting system, the contact angle frequently varies with chemical reaction and formation of a new solid compound at drop/substrate interface. The final contact angle is controlled by the new compound formed at the interface rather than by the initial substrate according to the RPC model [26,27]. Thus theoretically, the equilibrium contact angles of the Sn–3.5Ag–0.5Cu/Ni–P–(0,3,6)SiC coated SiC_p/Al systems should be almost the same since the compositions of “reaction products” (i.e., the interaction layers) are similar. However, an obvious difference among the final contact angles can be observed from the experiment results (Fig. 5). This discrepancy between the experiment results and the theoretical predictions can be resolved by considering the spreading kinetics of the molten drops on the Ni–P–(0, 3, 6)SiC coated SiC_p/Al substrates.

During the wetting process, a metastable configuration is established at the triple line where the extension of the molten drop is hindered by the presence of non-reactive SiC particles in front of the triple line. The change in surface energy ΔG of the system resulting from a small displacement Δx of the triple line is expressed as [34]

$$\Delta G = \Delta g_v \cdot e \cdot \Delta x + [\sigma_{SV}^0 - \sigma_{SL}^0 - \sigma_{LV}^0 \cos \theta(t)] \Delta x \quad (2)$$

where Δg_v is the Gibbs energy of the reaction per unit volume of product, e is the thickness of the reaction product, σ_{SV}^0 , σ_{SL}^0 and σ_{LV}^0 are the initial solid–vapor, solid–liquid and liquid–vapor surface energies,

respectively and $\theta(t)$ is the instantaneous contact angle on the reaction product surface.

As discussed above, the initial Ni–P(–SiC) surfaces are covered by the corresponding intermetallic compounds. Equation (1) can be written as

$$\Delta G = [\sigma_{SV}^0 - \sigma_{PL} - \sigma_{LV}^0 \cos \theta(t)] \Delta x \quad (3)$$

where σ_{PL} is the product–liquid surface energy.

The driving force $f_d(t)$, given by the change in the surface and interface energy ΔG of the system resulting from a lateral displacement of the triple line, is written as [34]

$$f_d(t) = -\frac{d(\Delta G)}{d(\Delta x)} = \sigma_{LV}^0 [\cos \theta_p - \cos \theta(t)] \quad (4)$$

where θ_p is the equilibrium contact angle of the molten drop on the reaction product surface.

Equation (4) describes the effect of driving force on the extension of the triple line. To overcome the barrier, the energy of the wetting system needs to increase with the increase of SiC content in the coating, although the change in Gibbs energy of the system due to the formation of new products is similar. This phenomenon can be demonstrated by the difference of the spreading rates of the various systems (Fig. 5). Therefore, the instantaneous increase in the contact angle with the SiC particle additions in the coating should be mainly attributed to the rise of the energy to overcome the wetting barriers (Fig. 8). A drop remains in a metastable state if it does not possess energy needed for overcoming the barrier between the state and the next one along the direction of stable equilibrium [34]. As a result, the spreading keeps going and cannot arrive at the equilibrium in the holding time of 30 min (Fig. 5).

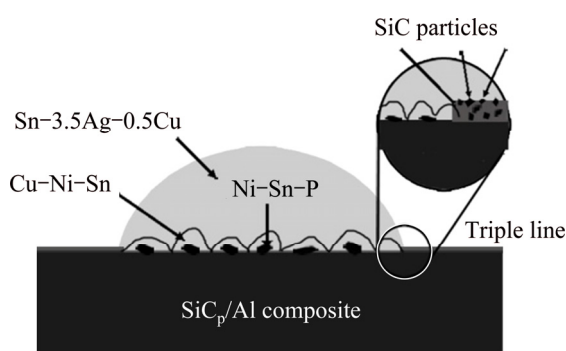


Fig. 8 Schematic diagram of triple line of wetting systems

4 Conclusions

1) The co-deposited SiC particles into the Ni–P coating affect the surface morphology of the coating, and enhance its surface roughness. No reaction layer is detected at the coating/substrate interfaces and the SiC

particles are evenly distributed in the coating and enveloped with nickel.

2) The SiC particle additions have a great effect on the wettability of the Sn–3.5Ag–0.5Cu/Ni–P(–SiC) coated SiC_p/Al system, that is, the final contact angle increases from 19° to 29°, 43° and 113° while holding for 30 min at 400 °C with the SiC concentration in the bath increasing from 0 to 3, 6, and 9 g/L.

3) For the Sn–3.5Ag–0.5Cu/Ni–P–(0,3,6)SiC coated SiC_p/Al systems, the Ni–P(–SiC) coating is completely dissolved in the drop after the wetting, resulting in formation of an interaction layer composed of Cu–Ni–Sn and Ni–Sn–P phases. While for the Sn–3.5Ag–0.5Cu/Ni–P–9SiC coated SiC_p/Al system, the interaction layer only consists of the Ni–Sn–P phase.

4) The increase of SiC particle additions in the Ni–P coating brings about the obvious variation of final contact angle, which can be mainly attributed to the increase of surface energy needed to overcome the wetting barriers, rather than the change in Gibbs energy of the system.

References

- [1] IBRAHIM I A, MOHAMED F A, LAVERNIA E J. Particulate reinforced metal matrix composites—A review [J]. *Journal of Materials Science*, 1991, 26(5): 1137–1156.
- [2] SURAPPA M K. Aluminum matrix composites: Challenges and opportunities [J]. *Sadhana*, 2003, 28(1–2): 319–334.
- [3] DAVIS L C, ARTZ B E. Thermal conductivity of metal–matrix composites [J]. *Journal of Applied Physics*, 1995, 77(10): 4954–4960.
- [4] WANG X H, NIU J T, GUAN S K, WANG L J, CHENG D F. Investigation on TIG welding of SiC_p-reinforced aluminum–matrix composite using mixed shielding gas and Al–Si filler [J]. *Materials Science and Engineering A*, 2009, 499(1): 106–110.
- [5] LU J B, MU Y C, LUO X W, NIU J T. A new method for soldering particle-reinforced aluminum metal matrix composites [J]. *Materials Science and Engineering B*, 2012, 177(20): 1759–1763.
- [6] LI L B, AN M Z. Electroless nickel–phosphorus plating on SiC_p/Al composite from acid bath with nickel activation [J]. *Journal of Alloys and Compounds*, 2008, 461(1–2): 85–91.
- [7] URENA A, UTRILLA M V, RAMS J, RODRIGO P, FERRER M. Electroless multilayer coatings on aluminum–silicon carbide composites for electronics packaging [J]. *Journal of the European Ceramic Society*, 2007, 27(13–15): 3983–3986.
- [8] ZHAO H F, TANG C M, LI C M, CHEN G C, LU F X, CAI Y H, GUO H, ZHANG R Q, ZHANG P W. Thermal conductive properties of Ni–P electroless plated SiC_p/Al composite electronic packaging material [J]. *Surface and Coatings Technology*, 2008, 202(12): 2540–2544.
- [9] SOLEIMANI R, MAHBOUBI F, ARMAN S Y, KAZEMI M, MANIEE A. Development of mathematical model to evaluate microstructure and corrosion behavior of electroless Ni–P/nano-SiC coating deposited on 6061 aluminum alloy [J]. *Journal of Industrial and Engineering Chemistry*, 2015, 23(25): 328–337.
- [10] MA C Y, WU F F, NING Y M, XIA F F, LIU Y F. Effect of heat treatment on structures and corrosion characteristics of electroless Ni–P–SiC nanocomposite coatings [J]. *Ceramics International*, 2014, 40(7): 9279–9284.
- [11] CALDERON J A, HENAO J E, GOMEZ M A. Erosion–corrosion resistance of Ni composite coatings with embedded SiC

- nanoparticles [J]. *Electrochimica Acta*, 2014, 124(1): 190–198.
- [12] GOU Yin-ning, HUANG Wei-jiu, ZENG Rong-chang, ZHU Yi. Influence of pH values on electroless Ni–P–SiC plating on AZ91D magnesium alloy [J]. *Transactions of Nonferrous Metals Society of China*, 2010, 20(S2): s674–s678.
- [13] ZHANG S S, HAN K J, CHENG L. The effect of SiC particles added in electroless Ni–P plating solution on the properties of composite coatings [J]. *Surface and Coatings Technology*, 2008, 202(12): 2807–2812.
- [14] WU Mao, QU Xuan-hui, HE Xin-bo, REN Shu-bin, QIN Ming-li. Interfacial reactions between Sn–2.5Ag–2.0Ni solder and electroless Ni(P) deposited on SiC_p/Al composites [J]. *Transactions of Nonferrous Metals Society of China*, 2010, 20(6): 958–965.
- [15] CHEN Z, HE M, QI G J. Morphology and kinetic study of the interfacial reaction between the Sn–3.5Ag solder and electroless Ni–P metallization [J]. *Journal of Electronic Materials*, 2004, 32(12): 1465–1472.
- [16] SHARIF A, ISLAM M N, CHAN Y C. Interfacial reactions of BGA Sn–3.5%Ag–0.5%Cu and Sn–3.5%Ag solders during high-temperature aging with Ni/Au metallization [J]. *Materials Science and Engineering B*, 2004, 113(3): 184–189.
- [17] LIN Y C, DUH J G, CHIOU B S. Wettability of electroplated Ni–P in under bump metallurgy with Sn–Ag–Cu solder [J]. *Journal of Electronic Materials*, 2006, 35(1): 7–14.
- [18] SATYANARAYAN, PARBHU K N. Wetting behaviour and interfacial microstructure of Sn–Ag–Zn solder alloys on nickel coated aluminium substrates [J]. *Journal of Materials Science & Technology*, 2011, 27(7): 1157–1162.
- [19] LUO W Q, LIU G W, ZHANG X Z. Microstructure, mechanical and thermal properties of Ni–P(–SiC) coating on high volume fraction SiC_p/Al composite [J]. *Rare Metals*, 2017. <https://doi.org/10.1007/s12598-017-0934-5>.
- [20] MALFATTI C F, FERREIRA J Z, OLIVEIRA C T, RIEDER E S, BONINO J B. Electrochemical behavior of Ni–P–SiC composite coatings: effect of heat treatment and SiC particle incorporation [J]. *Materials and Corrosion*, 2012, 63(1): 36–43.
- [21] MALFATTI C F, VEIT H M, MENEZES T L, FERREIRA J Z, RODRIGUS J S, BONINO J B. The surfactant addition effect in the elaboration of electrodeposited NiP–SiC composite coatings [J]. *Surface and Coatings Technology*, 2007, 201(14): 6318–6324.
- [22] SOLEIMANI R, MAHBOUBI F, ARMAN S Y, KAZEMI M, MANIEE A. Development of mathematical model to evaluate microstructure and corrosion behavior of electroless Ni–P/nano-SiC coating deposited on 6061 aluminum alloy [J]. *Journal of Industrial and Engineering Chemistry*, 2015, 23(25): 328–337.
- [23] CHANG C S, HOU K H, GER M D, CHUNG C K, LIN J F. Effects of annealing temperature on microstructure, surface roughness, mechanical and tribological properties of Ni–P and Ni–P/SiC films [J]. *Surface and Coatings Technology*, 2016, 288(25): 135–143.
- [24] WENZEL R N. Resistance of solid surfaces to wetting by water [J]. *Journal of Industrial and Engineering Chemistry*, 1936, 28(8): 988–994.
- [25] EUSTATHOPOULOS N. Progress in understanding and modeling reactive wetting of metals on ceramics [J]. *Current Opinion in Solid State and Materials Science*, 2005, 9(4): 152–160.
- [26] EUSTATHOPOULOS N. Wetting by liquid metals—application in materials processing: The contribution of the grenoble group [J]. *Metals*, 2015, 5(1): 350–370.
- [27] ALAM M O, CHAN Y C. Effect of 0.5 wt% Cu in Sn–3.5%Ag solder on the interfacial reaction with Au/Ni metallization [J]. *Chemistry of Materials*, 2003, 15(23): 4340–4342.
- [28] SHARIF A, ISLAM M N, CHAN Y C. Interfacial reactions of BGA Sn–3.5%Ag–0.5%Cu and Sn–3.5%Ag solders during high-temperature aging with Ni/Au metallization [J]. *Materials Science and Engineering B*, 2004, 113(3): 184–189.
- [29] WIERZBICKA-MIERNIK A, MIERNIK K, WOJEWODA-BUDKA J, LITYNSKA-DOBRYNSKA L, GARZEL G. Microstructure and chemical characterization of the intermetallic phases in Cu/(Sn,Ni) diffusion couples with various Ni additions [J]. *Intermetallics*, 2015, 59: 23–31.
- [30] CHEN G, WU F, LIU C, SILBERSCHMIDT V V, CHAN Y C. Microstructures and properties of new Sn–Ag–Cu lead-free solder reinforced with Ni-coated graphene nanosheets [J]. *Journal of Alloys and Compounds*, 2016, 656(25): 500–509.
- [31] KORHONEN T M, SU P, HONG S J, KORHONEN M A, LI C Y. Reactions of lead-free solders with CuNi metallizations [J]. *Journal of Electronic Materials*, 2000, 29(10): 1194–1199.
- [32] KUMAR G, PRABHU K N. Review of non-reactive and reactive wetting of liquids on surfaces [J]. *Advances in Colloid and Interface Science*, 2007, 133(2): 61–89.
- [33] EUSTATHOPOULOS N, NICHOLAS M G, DREVET B. Wettability at high temperatures [M]. Amsterdam: Pergamon, 1999.

Sn–3.5Ag–0.5Cu 在高体积分数 SiC_p/Al 复合材料 Ni–P(–SiC)镀层上的润湿性

张相召¹, 吴晓浪¹, 刘桂武¹, 骆文强¹, 郭亚杰², 邵海成¹, 乔冠军^{1,3}

1. 江苏大学 材料科学与工程学院, 镇江 212013;

2. 长安大学 材料科学与工程学院, 西安 710064;

3. 西安交通大学 金属材料强度国家重点实验室, 西安 710049

摘要: 基于化学镀 Ni 工艺, 研究 Sn–3.5Ag–0.5Cu 合金在 Ni–P(–SiC)镀层/SiC_p/Al 基体上的润湿行为, 分析镀层的显微结构和 Sn–3.5Ag–0.5Cu/Ni–P(–SiC)镀层/SiC_p/Al 体系的润湿和界面行为。结果表明, SiC 颗粒均匀地分布在镀层中, 且 Ni–P(–SiC)镀层与 SiC_p/Al 复合材料之间没有界面反应。Sn–3.5Ag–0.5Cu 对 Ni–P、Ni–P–3SiC、Ni–P–6SiC 和 Ni–P–9SiC 镀层/SiC_p/Al 基体对应的最终接触角分别为~19°、29°、43°和 113°。在 Sn–3.5Ag–0.5Cu/Ni–P(–0,3,6)SiC 镀层/SiC_p/Al 界面处形成含有 Cu、Ni、Sn 和 P 的反应层, 其主要包含 Cu–Ni–Sn 和 Ni–Sn–P 相。此外, 熔融的 Sn–Ag–Cu 合金可以通过 Ni–P/SiC 界面渗入 Ni–P(–SiC)复合镀层与 SiC_p/Al 基体接触。

关键词: Ni 镀层; Sn–Ag–Cu 合金; SiC_p/Al 复合材料; 润湿; 显微结构; 界面